J Therm Anal Calorim (2009) 98:611–622
DOI 10.1007/s10973-009-0505-6

The role of multi-walled carbon nanotubes in shear enhanced crystallization of isotactic poly(1-butene)

Rossana Iervolino · Elvira Somma · Maria Rossella Nobile · Xuming Chen · Benjamin S. Hsiao

Rheological Analysis of Polymers/Special Chapter

Abstract The flow-induced crystallization behavior of nanocomposites, containing isotactic poly(1-butene) (PB) and functionalized multi-walled carbon nanotubes (MWNT), was investigated. Three different MWNT concentrations (0.1, 1, 5 wt%) were used to prepare the nanocomposites. Effects of MWNT and shear flow on the crystallization parameters were evaluated separately. Rheological measurements based on oscillatory shear revealed induction time and crystallization half-time at the quiescent state, where both parameters exhibited the nucleating effect of MWNT on PB. Rheological measurements based on steady-state shear flow and short-time shear flow revealed the evolution of molecular orientation, which was studied in both PB and its nanocomposites. A small increase in crystallization kinetic was recorded in PB under shear having moderate values of the Weissenberg (*We*) number. On the other hand, a dramatic synergistic effect of MWNT and shear was detected under the same shear conditions for nanocomposites. The optical microscopic images exhibited a clear transition from isotropic to row-like morphology in the case of nanocomposites under shear.

Keywords Crystallization · Carbon nanotubes · MWNT · Rheology · Shear flow

R. Iervolino · E. Somma · M. R. Nobile (✉)
Dipartimento di Ingegneria Chimica e Alimentare,
Università degli Studi di Salerno, via Ponte don Melillo,
84084 Fisciano, SA, Italy
e-mail: mrnobile@unisa.it

X. Chen · B. S. Hsiao
Department of Chemistry, Stony Brook University,
Stony Brook, NY 11794-3400, USA

Introduction

The flow-induced crystallization behavior has long been considered relevant in controlling the final properties of semi-crystalline polymers in industrial processing because this behavior can affect the overall kinetics and morphology of the resulting product [1, 2]. In most polymer processing operations, the melts undergo both elongational and shear deformations. Although the latter has been considered as a weak flow, it is now well-established that even the application of a low intensity shear field to an undercooled polymer melt can significantly enhance the overall crystallization kinetics. The process can be attributed to the increase in nucleation as compared with crystallization in the quiescent state. Flow-induced structural changes during crystallization, such as the shear-induced shish-kebab formation, can be attributed to the stretching and aligning of polymer chains prior to crystallization [3–8].

Recently, several studies have become available in the literature that deal with the effects of processing parameters (e.g., shear rate and shear strain) and molecular properties of the polymer (e.g., molecular weight, molecular mass distribution, and fillers and nucleating agents) on flow-induced crystallization [2, 3, 9–23]. One key factor governing the orientation-induced crystallization is the relaxation behavior of polymer chains. Shear rate, of course, must be high enough to orient and align polymer chains in the melt to form stable nuclei. The stability of resulting orientation-induced nuclei also depends on the level of deformation (strain) on the sample (at low strains, the orientation and alignment of polymer chains may not be sufficient to form nuclei). A critical shear strain (at constant shear rate) or a critical shear rate (at a constant shear strain) is necessary to be overcome in order to enhance the nucleation and thus shorten the crystallization time after flow. To study strain as a parameter for

shear-induced crystallization, Janeschitz-Kriegl and coworkers [24] have demonstrated a short-time shearing protocol technique, at which the undercooled melt is sheared in isothermal conditions for a short time. This technique enables the separation of flow, nucleation, and growth phenomena, where the shear strain is imposed on the melt at the very onset of the experiment to define the initial condition of the crystallization. The short-time shearing technique has been adopted by several different research groups to reveal the shear and strain effects on the crystallization process, mostly under simple shear conditions [2, 3, 9–18].

The parameter of molecular weight also plays an important role on flow enhanced crystallization. Longer polymer chains often become more oriented than shorter chains after deformation since the former possess longer relaxation times. In polydisperse polymers, Keller proposed that at a given shear rate, only those molecules having molecular weights above a critical value can form stable oriented nuclei after deformation, whereby this behavior has been recently verified in polymer melts by Hsiao and coworkers [10, 25] under shear flow by using rheo-X-ray techniques. They [6, 26] also suggested that it is unlikely that the coil-stretch transition can take place at the level of individual chain due to the large number of chain entanglements in high molecular weight polymer melts. The results reported for the sheared polyethylene (PE) blend with 2% of ultrahigh molecular weight polyethylene (UHMWPE) [5] clearly showed, for the extracted UHMWPE, that the coil-stretch transition occurred only in sections between the kebabs, indicating a deformed but still entangled melt. In flexible polymer melts without fillers, the initially formed precursor structure can consist of shish-kebab entities with multiple short length shish that can incorporate the entanglement points as defects in the shish assembly.

In recent articles, the filler effect on the crystallization kinetics has been studied [21, 22, 27–32]. For example, the inclusion of carbon nanotubes has been found to increase the overall crystallization kinetics [27–30]. In the case of aramid fiber/isotactic polypropylene composites [32], the combined effect of shear and fibrous filler was found to be synergistic instead of additive in terms of the total degree of crystallinity, the nucleation, and crystallization rates. In this article, the flow-induced crystallization behavior of nanocomposites with multi-walled carbon nanotubes (MWNT) was investigated. Isotactic poly(1-butene) (PB) was used as the polymer matrix in nanocomposites. PB turns out to be a good model system for study of flow-induced crystallization, due to its relatively slow crystallization kinetics at low to moderate degrees of undercooling [14–16, 33–38]. This polymer, first synthesized by Natta and coworkers [39], has excellent mechanical properties. However, despite the potentiality, its production is relatively restricted, while one of the main reasons, beside the high cost of the monomer, is related to its peculiar crystallization characteristics. In particular, PB has a very complex polymorphic behavior and can crystallize into five different crystalline phases, corresponding to different modes of chain packing. The most common and important crystalline phases are identified as Form I, Form II, and Form III. Melt crystallization of PB in quiescent condition at atmospheric pressure usually produces tetragonal Form II, which is kinetically favoured [39, 40]. Form II, on storage at room temperature after approximately 10 days, converts to Form I, in which crystalline strands adapt to slightly extended 3/1 helix [41, 42]. In this article, our results only revealed the Form II structure, which is consistent with that obtained from melt crystallization of PB.

The aim of this work is to obtain some new insight into the role of MWNTs (in the flow-induced crystallization of nanocomposites). To reach this aim, nanocomposites based on isotactic PB with different content of MWNT were investigated by mean of rheological measurements performed in the low shear rate region. In the first part of this study, the quiescent crystallization behavior was investigated and the results were used as the reference point for the study of the flow-induced crystallization. In the second part of the study, short-time shear experiments, in which the shear parameters (shear rate and shear strain) were varied independently, were carried out. To gain indication of molecular orientation during shear flow, a parallel superposition of steady flow and dynamic conditions was also performed. It was found that such rheological measurements are particularly suitable to determine the effects of shear and MWNT on the overall crystallization behavior and the results clearly showed the two effects are synergistic. To monitor the morphological changes in nanocomposites, rheo-optical experiments during isothermal crystallization process in quiescent and shear flow conditions were also performed.

Experimental

Materials

The isotactic PB sample used in this work, named PB400, was kindly supplied by Basell Polyolefins in the form of pellets, without nucleating agents. Alfonso and coworkers [43] studied the polymorphism of isotactic PB. The value of the thermodynamic melting temperature of Form II, $T_m^{0(II)} = 134$ °C for the PB400 sample has been kindly provided by Prof. Alfonso, based on the method suggested by Marand [44, 45], and it is reported in Table 1. The nominal melting

Table 1 Physical properties of the pure PB400

Polymer	M_n	M_w	M_w/M_n	M_z/M_w	$T_m^{0(II)}$
PB400	54,000	177,000	3.3	2.30	134 °C

temperature (T_m) values typically observed in DSC heating runs were in the range 110–120 °C for Form II, whereas the values in the range 120–135 °C were often reported for the melting of Form I [46]. A summary of the sample molecular parameters, as obtained from GPC measurements are reported in Table 1.

The PB400 sample was used as the polymer matrix for preparation of PB/MWNT nanocomposites. Nanocomposites with three different amounts (0.1, 1, 5 wt%) of functionalized multi-walled nanotubes (MWNT) were prepared; they were named as 0.1PB400, 1PB400, and 5PB400, respectively. The MWNTs were provided by the Nanostructured and Amorphous Materials, Inc.. They were produced by catalytic chemical vapor deposition method. The diameter of the MWNTs was about 8–15 nm and the length of MWNT was in the range of a few micrometers. The aspect ratio (L/D ratio) was estimated to be 500–1000. According to the manufacturer's specification, the purity of the raw MWNTs was more than 95%.

As-received MWNTs were oxidized using a mixture of concentrated H_2SO_4/HNO_3 in 3:1 ratio to generate surface acidic groups. In the oxidation processes, 0.5 g of MWNT was suspended in 50 mL of a 3:1 mixture containing concentrated H_2SO_4 (98 wt%)/HNO_3 (16 M). The mixture was sonicated in water bath for 3 h, immediately followed by 18 h of equilibration at 34 °C. In order to obtain functionalized MWNT, the oxidized MWNTs were dispersed in octadecylamine at 70 °C and maintained at 180–190 °C under nitrogen for 24 h. The resulting suspension was washed with chloroform and alcohol several times, and was then filtered with a 0.1-μm pore membrane under vacuum.

By solution blending method, the PB/MWNT nanocomposites were prepared. The detailed preparation procedure was as follows.

- The surface modified MWNTs were first added in xylene to obtain a concentration of approximately 2.5 mg/mL. The suspension was vigorously stirred in an ultrasonic bath until there was no visible precipitation of MWNT.
- An appropriate amount of PB was dissolved in 180 mL xylene at 140 °C to obtain a homogenous polymer solution.
- The modified MWNT/xylene solution was then slowly added into the above polymer solution and the resulting mixture was kept at 140 °C for 30 min under stirring.
- Precipitation of the MWNT/polymer solution was carried out by pouring it into cold methanol (5–6 times the original volume of xylene in the MWNT/polymer solution) under continuous stirring.
- The MWNT/polymer blend slurry was filtered from xylene and methanol mixture, dried extensively at room temperature, and then subsequently annealed at 70 °C in a vacuum oven for 2 days to yield nanocomposites.

Methods

Rheological measurements

The crystallization process has been monitored by means of rheological experiments, which can be described as follows. The measurements for isothermal crystallization of PB400 neat resin as well as 0.1PB400, 1PB400, and 5PB400 nanocomposites, were performed by the rotational stress rheometer, SR5000 (Rheometric Inc.), in a cone-and-plate configuration ($D = 25$ mm, the cone angle $\alpha = 0.1$ rad), under nitrogen atmosphere. The cone-and-plate configuration guarantees that the whole sample was subjected to a uniform shear rate. The following thermo-mechanical history was used in all rheological crystallization experiments (i.e., quiescent tests and step-shear flow tests).

- The annealing treatment was realized at T_A=180 °C for 10 min to erase any crystallinity that could affect the subsequent crystallization process.
- The cooling step from 180 °C to the crystallization temperature was performed with a rate of 10 °C min^{-1}. The temperature profile was verified by a thermocouple placed inside the molten sample between the tools.
- The isothermal crystallization kinetics at $T_c = 95$ °C was studied.

To follow both cooling and isothermal crystallization processes, the evolution of the storage modulus, G', was monitored by an oscillatory test at the constant stress of 1,000 Pa and a constant frequency of 1 rad s^{-1}. The choice of the values for these parameters was crucial in order to minimize the disturbance during crystallization, which has been discussed in detail in previous works [14, 33]. The storage modulus represents, therefore, our probe to follow the crystallization process.

In the case of the quiescent crystallization study, the kinetic results was reported in terms of a rheological induction time, t^{Q}_{onset} (i.e., quiescent induction time), defined at the time where the storage modulus increases of about 10% of its initial value measured at the crystallization temperature of 95 °C. To determine t^{Q}_{onset}, the cooling time needed to be subtracted; therefore, this time was counted from the instant where the crystallization temperature was reached; i.e., only the isothermal process was considered. Moreover, the overall kinetics of the process was also evaluated by the "rheological half-time," $t^{Q}_{0.5}$, defined as the time when the storage modulus reached its half level between the initial and final values, as measured at $T_c = 95$ °C. Analogously to the determination of t^{Q}_{onset}, in the evaluation of $t^{Q}_{0.5}$, the cooling time was also subtracted and the zero time scale was fixed at the end of the cooling step. The overall crystallization rate, k^{Q}, was evaluated as the inverse of $t^{Q}_{0.5}$, which has been previously

reported [14, 33, 47]. The superscript "Q" defines the quiescent crystallization experiments.

To investigate the influence of a shear flow on the isothermal crystallization process, continuous shear flow crystallization experiments were also carried out at $T_c = 95$ °C (Fig. 1a). In this study, shear flow was applied at different shear rates, where the evolution of viscosity (and/or steady stress) during the shear flow was monitored. The abrupt increase in the viscosity profile represented the onset of the crystallization process. The rheological induction time for the isothermal crystallization process at 95 °C under continuous shearing, t^{CS}_{onset}, was determined as the time where the viscosity increased 10% of its initial value (the cooling time was subtracted while only the isothermal process was considered). The t^{CS}_{onset} value represented the maximum shear time that could be adopted during the step-shear deformation before crystallization starts.

Short-time shear-induced crystallization experiments in simple shear flow have also been performed. In this case, the step-shear flow, contrary to the continuous shear flow crystallization experiments, was only applied for a limited period of time, never exceeding the maximum shear time evaluated in the continuous shear flow experiments. To achieve the aim to gain insight into molecular orientation, the storage modulii after shear flow (that could allow us to understand its effect on crystallization kinetics as reported in previous articles [14, 33, 47]) as well as during shear flow were measured by a parallel superposition of steady flow and dynamic conditions as illustrated in Fig. 1b. This parallel superposition experiments in a stress-controlled rheometer revealed the shear stress as a result of two contributions: a constant value and a sinusoidal contribution [48]. Typically, the rheometer measures the resulting deformation, e.g., the storage and loss compliances (after an initial transient), which can be "converted" into storage and loss modulii by using the classical modulus–compliance relationships in the linear viscoelastic regime [49]. In the following, the parallel storage modulus measured during flow will be indicated, for simplicity, always as G'.

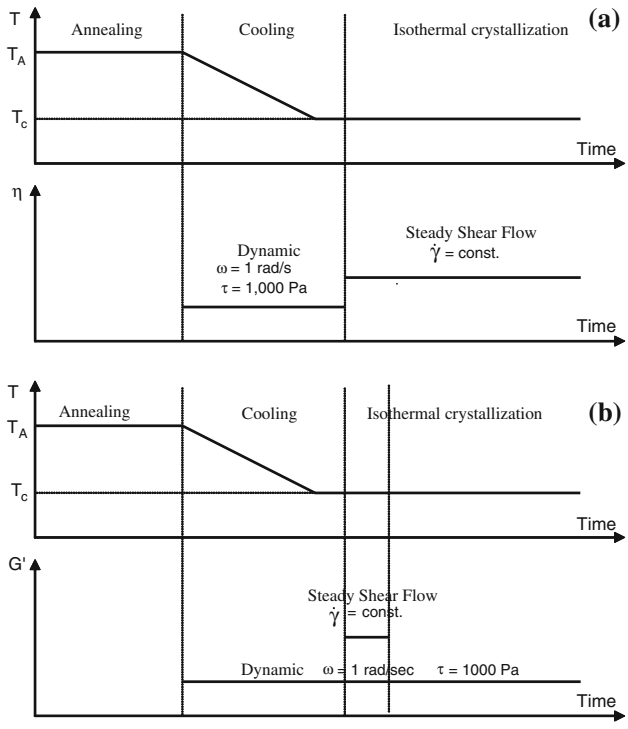

Fig. 1 **a** Schematic drawing of a continuous shear flow crystallization test. **b** Schematic drawing of a step-shear flow crystallization test

The step-shear (SS) flow was carried out as soon as the crystallization temperature was reached. Different shear rates were applied with the constraint of a constant shear strain $\gamma = \dot{\gamma} t_s$ (t_s = shear time), where different shear times were used. The shear strain was kept at a constant value of about 20 shear unit. The kinetic results of the crystallization process have been estimated from the rheological induction time and the "rheological half-time," $t^{SS}_{0.5}$, as defined earlier. The overall crystallization constant (k_{SS}) was calculated and the kinetic parameter, k_{SS}/k_Q, defined as the "flow sensitivity," was used to quantify the crystallization kinetics in step-shear study.

Optical measurements

The evolution of crystalline morphology was observed by a polarizing optical microscope (Universal polarizing microscope BX41, Olympus) equipped with a CCD camera, different magnification objectives, and a shear stage (CSS 450 of Linkam Scientific Instruments). The optical microscopic images were collected by a frame grabber (DT-3152, Data Translation Inc). The quantitative analysis of the digital images was carried out by suitable image analysis software (Analysis FIVE, Olympus software).

A sample thickness of 100 μm was chosen as a good compromise between the opposite needs of clear optical observation of growing spherulites and of experimental conditions close to those used in the rheological measurements. The thermo-mechanical protocol applied in this study was similar to that of the rheological measurements.

Results and discussion

Isothermal quiescent crystallization study

Typical rheological curves collected during isothermal quiescent crystallization conditions are shown in Fig. 2. This figure illustrates the evolution of storage modulus, G', as a function of time at $T_c = 95$ °C for nanocomposite with

5 wt% of MWNT (5PB400) in two repeated runs performed under the same conditions. The results of the quiescent crystallization experiments performed in the stress rheometer show a good reproducibility. In this figure, the evolution of G' versus time during the cooling stage from $T_A = 180$ °C as well as the subsequent isothermal crystallization at $T_c = 95$ °C is reported. The experiments show that the storage modulus is very sensitive to the structural changes during to crystallization. After the first increase in G', recorded during the cooling step, a plateau G' value at T_c is observed. The second growth of the modulus, representative of the crystallization process, is seen after the rheological quiescent induction time, t^{Q}_{onset}. Finally, a second plateau G' value is reached at the end of the crystallization process. It is noteworthy that in the analysis of the crystallization kinetics, the cooling time has been subtracted and only the isothermal process was considered, as it has been described in the rheological experimental section. Therefore, to evaluate both the quiescent induction time and the overall kinetics of the process, the zero time scale is fixed at the end of the cooling step, as shown in Fig. 2.

Up to now, no definitive ways to express the kinetics of the crystallization process from rheological experiments can be concluded in the literature. In order to quantitatively describe the crystallization behavior, we have estimated the overall kinetics of the process from a "rheological half-time," $t_{0.5}$, defined as the time where the storage modulus reaches half of its level between the initial and final values. The rheological response in the later stages of crystallization is dominated by percolation-induced structure formation leading to a rapid change of modulus and to extremely high values of the Avrami n exponent [50]. In general, the "rheological half-time," $t_{0.5}$, does not have the direct relationship with the relative degree of crystallinity of 0.5. However, it has been shown that the half-times measured from rheology and calorimetry could be comparable if the strain amplitude and the frequency of the oscillation were properly chosen (i.e., to obtain the linear viscoelastic behavior without perturbing the crystalline structure development) [36, 51], or in highly structured materials [50]. In the framework of this study, we have investigated the quiescent crystallization with properly chosen strain amplitude and frequency in order to determine the "reference" condition necessary to estimate the effect of the shear flow on the crystallization kinetics. We consider the quiescent "rheological half-time," $t^{Q}_{0.5}$, obtained from the G' data, as the "internal reference."

In Fig. 3, the evolution of the storage modulus, G', as a function of time during both the cooling process and the isothermal quiescent crystallization at $T_c = 95$ °C is reported for PB400/MWNT nanocomposite and the pure PB400 samples. The "rheological quiescent induction times" values, t^{Q}_{onset}, for these samples are reported in Table 2, which also illustrates the corresponding "rheological half-time," $t^{Q}_{0.5}$ values. The results clearly show the accelerating effect of the nanotubes on the crystallization kinetics with the increase in the MWNT content. Such behavior confirms the strong nucleating effect of the nanotube on the crystallization kinetics of PB [27–29].

It is noteworthy to mention that the percolation threshold of the PB400/MWNT composites at temperatures of 120 and 180 °C has been previously estimated from the rheological data of the composite melt [52]. As the nanotube content increases, the CNT–polymer–CNT interactions begin to dominate and, once the critical content of CNTs is reached, the formation of a CNT–polymer network can occur with marked alterations in dynamic moduli

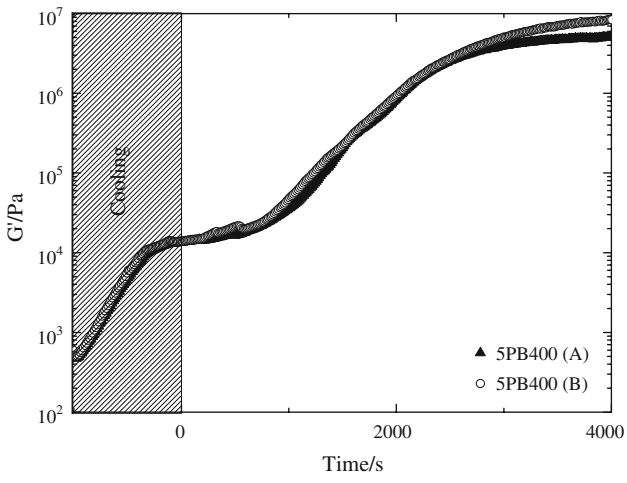

Fig. 2 Reproducibility of two quiescent crystallization experiments of 5PB400 nanocomposite at $T_c = 95$ °C

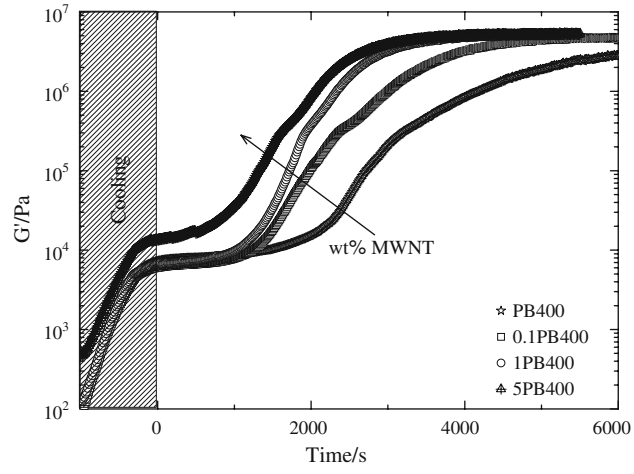

Fig. 3 Evolution of the storage modulus (G') during the cooling and the quiescent isothermal crystallization at $T_c = 95$ °C for the PB400/MWNT nanocomposites and the pure PB400

Table 2 Kinetic parameters for the quiescent isothermal crystallization of the PB400/MWNT nanocomposites and the pure PB400

Sample	t^{Q}_{onset}/s	$t^{Q}_{0.5}$/s
PB400	984 ± 98	4973
0.1PB400	750 ± 75	3644
1PB400	555 ± 55	2795
5PB400	316 ± 32	2531

$T_c = 95$ °C

and viscosity (showing a liquid like–to-solid like transition). This critical composition is denoted as the "rheological percolation threshold." The interconnected structure influences the relaxation phenomena of the polymer chains. In literature, the plateau value in G', exhibited by nanocomposites at lower frequencies above a critical concentration, was interpreted as the occurrence of the rheological percolation threshold [53–55]. Pötschke et al. [54] suggested a plot of the phase angle (δ) against the complex modulus, G^* (van Gurp–Palmen plot) to identify the rheological percolation threshold. This transition can also be interpreted in terms of a physical gelation process, as demonstrated by different authors [56, 57].

In the PB400/MWNT composites at $T = 180$ °C, a value of ~0.5 wt% for the rheological percolation threshold has been evaluated from both the van Gurp–Palmen plot as well as the Winter and Chambon method [52]. Moreover, it was found that this value increased to ~2.5 wt% at $T = 120$ °C. The rheological percolation threshold is temperature-dependent, as reported in the literature [54, 58]. However, it was also shown that the storage and loss modulii of the pure matrix were not modified when 0.1 wt% of MWNT was added to the PB matrix at $T = 120$ °C [52]. It can be, therefore, assumed that the undercooled melts of PB400/MWNT nanocomposites with content of 0.1 and 1 wt% of carbon nanotube are below the percolation threshold at the temperature of 95 °C.

The optical micrographs taken during the isothermal crystallization at $T = 95$ °C for the PB400 matrix as well as the 0.1PB400 and 1PB400 MWNT nanocomposites are shown in Fig. 4a–c, respectively. In the case of the PB400 matrix, the optical microscopy image exhibits typical Maltese-cross spherulitic features, indicating the presence of isotropic spherulites, and a very sporadic nucleation even after 1,200 s. It has been known that isotactic PB isothermally crystallized from the melt can exhibit either spherical crystallites and/or square-shaped crystallites [35, 59], depending on the crystallization temperature and molecular weight. The latter morphology has been called "hedrites" by Strobl and co-workers [59] as they resembled single crystals obtained from solution. The pure PB400 matrix ($M_w = 177{,}000$) crystallized at the temperature of 95 °C

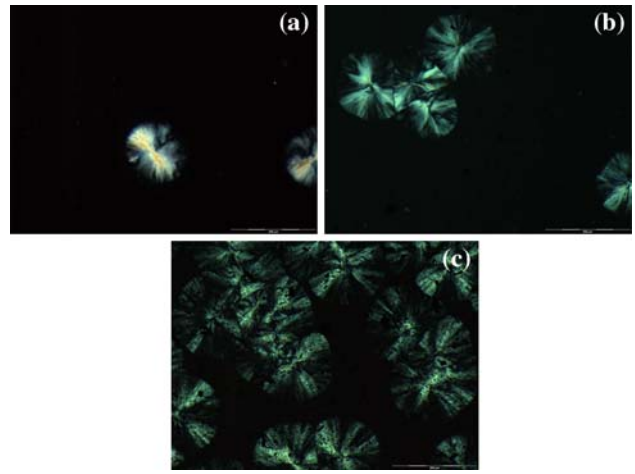

Fig. 4 Optical microscopy images during quiescent crystallization at $T_c = 95$ °C. **a** PB400, **b** 0.1PB400, and **c** 1PB400. The micrographs refer to a crystallization time of 1,200 s. The length of the scale bar is 200 μm

shows only the spherical crystallites, in agreement with literature findings [35, 59]. In contrast to the pure matrix, the micrographs in Fig. 4b, c show that the inclusion of nanotubes hinders the formation of ordered crystallites (this is particularly evident in the case of 1PB400 nanocomposite). Moreover, with the increase in the MWNT content, the density of spherulites increases significantly, indicating the strong effect of nanotubes in promoting the nucleation of the crystallizing PB matrix. This finding confirms the rheological results.

Flow-induced crystallization

This section intends to deal with combined role of shear flow and carbon nanotubes inclusion on the isothermal crystallization kinetics of the PB400/MWNT nanocomposites by means of rheological measurements performed in the low-shear rate region. The results from the nanocomposite made with the lowest content of carbon nanotube were discussed, since in this case the presence of the very little amount of filler is not expected to modify the flow behavior of the pure PB matrix. The subsequent crystallization process thus can clearly reveal whether the combined effect of flow and carbon nanotube filler is additive or synergistic.

In Fig. 5, the flow curves for the pure PB400 and 0.1PB400 nancomposite samples are reported at the isothermal temperature $T_c = 95$ °C, after cooling from the annealing treatment at $T_A = 180$ °C. Before the crystallization process sets in, the samples remain essentially in the state of an undercooled melt at $T_c = 95$ °C, where the corresponding viscosity values can be measured. It is seen that the flow curves for the PB400 matrix and the 0.1PB400

nanocomposite are nearly identical. Furthermore, the Newtonian and shear thinning regions occur at similar shear rates for the pure PB matrix and the 0.1PB400 nanocomposite. At the chosen experimental shear rates, the coupling effects between the flow intensity and the relaxation behavior of polymer chains seem to produce a similar degree of orientation during flow for both pure PB and 0.1PB400 nanocomposite samples, where the latter contained a very low percentage of nanotube (0.1 wt% of MWNT) well below the percolation threshold.

The relaxation behavior of the polymer melt can be described in terms of a characteristic relaxation time [8, 12, 13, 15, 60, 61]. The longest relaxation time, i.e., the disengagement time of the macromolecules (τ_d) can be clearly defined and used to characterize a narrow distribution of molecular weight. With the broadening of the molecular weight distribution, such a relaxation time cannot be well defined but a longest relaxation time can be estimated as the inverse of the critical shear rate at the onset of shear thinning in the flow curve. This time was used to represent the characteristic relaxation time (τ_η) of the system in this study. As it is shown in Fig. 5, the viscosity starts to decrease at $\sim 0.1\ s^{-1}$, which corresponds to $\tau_\eta \sim 10$ s for the undercooled PB400 matrix at $T = 95$ °C. To confirm this estimate, we have also fitted dynamic data previously published [33] with the BSW-GEX model described in a recent article [62] and the results are as follows. If a well-behaved relaxation spectrum is obtained over a large time range, then reliable rheological constants, i.e., the zero shear rate viscosity and the steady-state compliance, can be computed using the sum rules on the evaluated relaxation spectrum. Thus, the average longest relaxation time can be estimated as the zero shear rate viscosity times the steady-state compliance. Using this method, the calculated average longest relaxation time yields a value of 5.7 s, which is in good agreement with the estimated value based on the flow curve.

Flow-induced crystallization tests under short-time simple shear conditions with parallel superposition of steady flow and dynamic conditions have also been performed. Such measurements are a useful tool to determine the individual *versus* the combined role(s) of molecular orientation during flow and the inclusion of carbon nanotube in enhanced nucleation. A direct comparison of G' profiles for the PB400 and 0.1PB400 samples during the step-shear at a shear rate of $0.3\ s^{-1}$ (i.e., in the shear thinning region) and a shear time of 70 s as well as the subsequent crystallization process, is shown in Fig. 6a, b, respectively. As expected, in both samples, a decrease in G' during the application of the shear flow is seen. This finding is in agreement with the flow curves results (Fig. 5), where the magnitude of the decrease is similar for

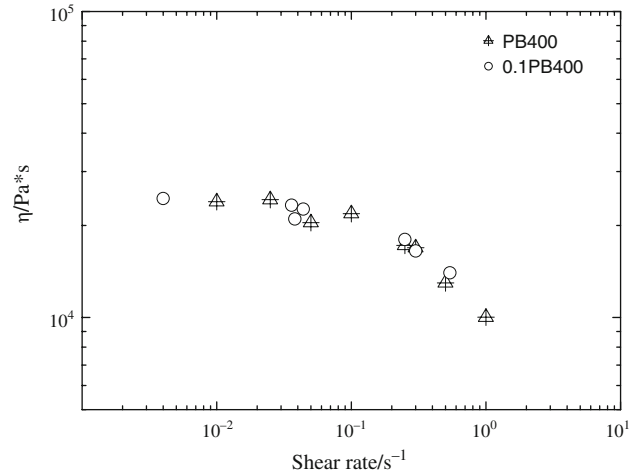

Fig. 5 Flow curve, viscosity (η) versus shear rate, of the pure PB400 and the 0.1PB400 nanocomposite. $T_c = 95$ °C

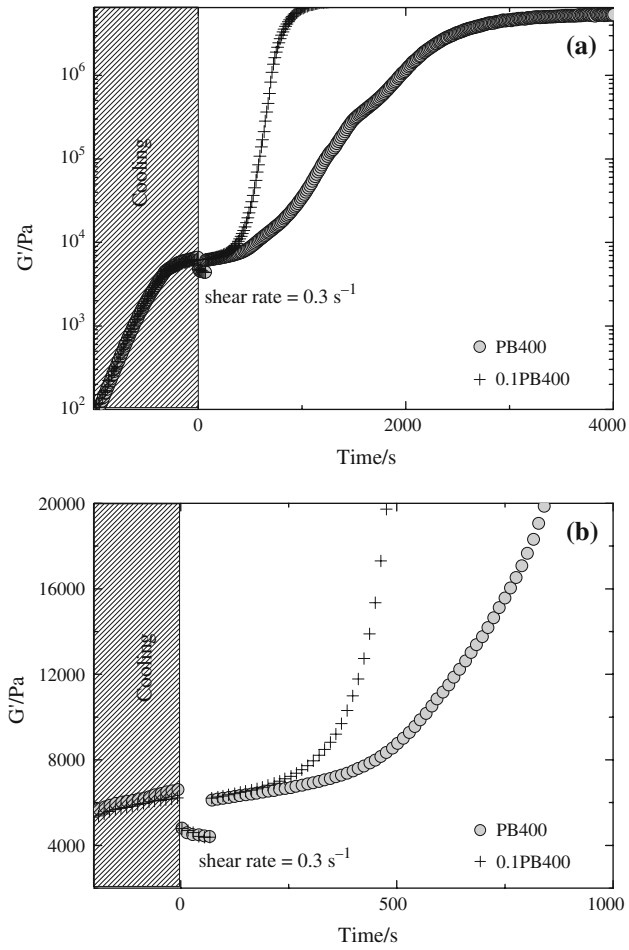

Fig. 6 **a** Storage modulus (G') versus time for the pure PB400 and the 0.1PB400 nanocomposite during the step-shear crystallization experiment with shear rate = $0.3\ s^{-1} \times 70$ s. $T_c = 95$ °C. **b** Storage modulus versus time, during the early stages of the step-shear crystallization experiment

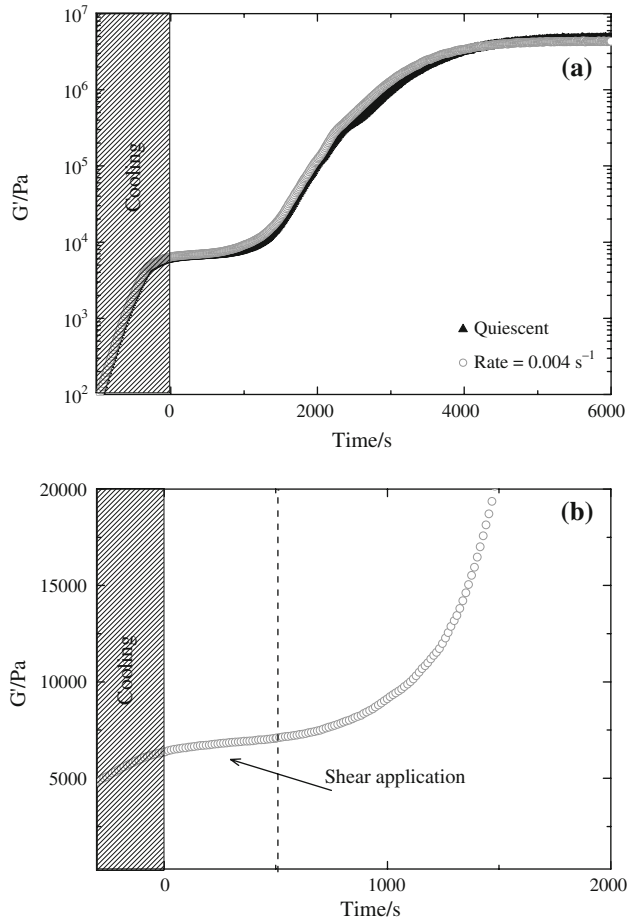

Fig. 7 **a** Storage modulus (G') versus time for the 0.1PB400 nanocomposite during the quiescent and step-shear crystallization experiment with shear rate=0.004 s^{-1} × 500 s. T_c = 95 °C. **b** Storage modulus versus time, during the early stages of the step-shear crystallization experiment

both 0.1PB400 nanocomposite and PB samples (Fig. 6b). This suggests that both samples have a similar degree of molecular anisotropy. Nonetheless, the nanocomposite sample shows a much faster subsequent crystallization rate due to the presence of carbon nanotubes in the crystallization process (Fig. 6a).

In Fig. 7a, b, the evolution of G' over time for the 0.1PB400 nanocomposite sample in a step-shear crystallization test at a shear rate in the Newtonian region ($\dot{\gamma} = 0.004$ s^{-1}) is shown, where the results are also compared to the corresponding evolution of G' at the quiescent state. In this case, no decrease in G' is observed during flow (i.e., the same value was also observed in the unperturbed state) (Fig. 7b); the crystallization kinetics after flow appears the same as that under the quiescent condition (Fig. 7a). This indicates that the applied shear rate is not strong enough to influence the crystallization in the nanocomposite melt. The flow-induced crystallization results for the

Table 3 Kinetic parameters of the pure PB400 and 0.1PB400 nanocomposite calculated from the step-shear flow tests

shear rate/s^{-1}	$t_{0.5}^{SS}$/s	k_{SS}/s^{-1}	k_{SS}/k_Q
Pure PB400			
2.30 × 10^{-2}	4822	2.07 × 10^{-4}	1.03
1.20 × 10^{-1}	4328	2.31 × 10^{-4}	1.15
2.50 × 10^{-1}	3648	2.74 × 10^{-4}	1.36
3.00 × 10^{-1}	3523	2.84 × 10^{-4}	1.41
5.1 × 10^{-1}	2408	4.15 × 10^{-4}	2.07
0.1PB400 nanocomposite			
4.00 × 10^{-3}	3395	2.95 × 10^{-4}	1.08
4.40 × 10^{-2}	2564	3.90 × 10^{-4}	1.42
2.55 × 10^{-1}	815	1.23 × 10^{-3}	4.48
3.00 × 10^{-1}	770	1.3 × 10^{-3}	4.74
5.20 × 10^{-1}	646	1.55 × 10^{-3}	5.65

T_c = 95 °C

0.1PB400 nanocomposite and the pure PB400 samples in different step-shear flow experiments are summarized in Table 3, in terms of the crystallization "rheological half-time," $t_{0.5}^{SS}$, and of the overall crystallization constant (k_{SS}).

The effect of flow on the crystallization kinetics can be discussed in terms of the dimensionless Weissenberg number ($We = \dot{\gamma}\tau_d$,) which has been demonstrated in the literature [8, 12, 13, 15, 16, 26, 61, 63]. If the *We* number is higher than 1, the flow time ($1/\dot{\gamma}$) becomes smaller than the disengagement time and chain segment orientation can take place. It has been shown that shearing at *We* slightly higher than 1 can readily result in an increase of nucleation density, and thus enhance the crystallization rate, shearing at $We \gg 1$ can give anisotropic growth of crystal structures [7, 8, 12, 13, 15, 16, 26]. Nevertheless, it is important to point out that only when the strain is kept constant, the *We* criterion can be used to determine the flow-induced crystallization kinetics. This is because the Weissenberg number does not capture the relaxation process after the cessation of flow [12].

Based on our findings reported above, the characteristic relaxation time (τ_η) for the PB400 matrix is ~10 s. This value is comparable to the value of 5.7 s obtained from the BSW-GEX model. From our results reported in Figs. 5 and 6 as well as in Table 3, we can see that the enhancement of the crystallization kinetics indeed takes place for *We* higher than 1. For example, at the shear rate of 0.3 s^{-1} (and a strain of 21), corresponding to the *We* value between 1.71 and 3.0, an increase in the crystallization kinetics is seen. The good correlation between the *We* number and the crystallization rate can be attributed to the fact that the shear influence is crucial at the beginning of the crystallization process, probably mainly through enhanced nucleation [12, 16, 26, 37].

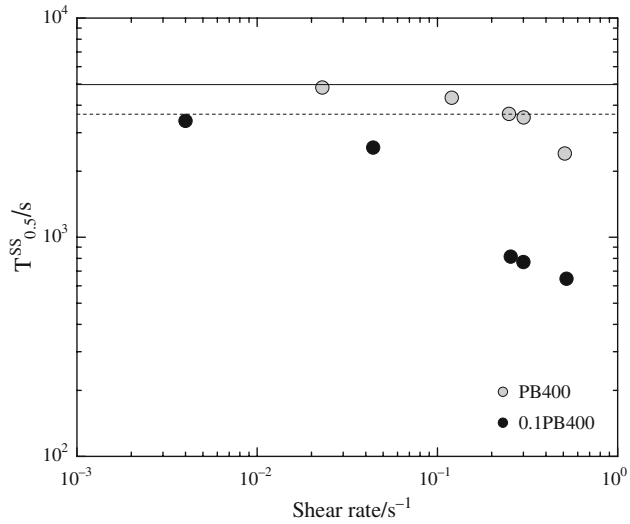

Fig. 8 The half crystallization time, $t^{SS}_{0.5}$, as a function of the shear rate for the pure PB400 and the 0.1PB400 nanocomposite. $T_c = 95$ °C. The horizontal lines correspond to quiescent conditions (continuous line for pure PB400 and dashed line for 0.1PB400 nanocomposite)

In order to evidence the enhanced crystallization behavior of the 0.1PB400 nanocomposites under step-shear flow, the "rheological half-time," $t^{SS}_{0.5}$, values are reported against the shear rate for both PB400 and 0.1PB400 nanocomposite samples (Fig. 8). The corresponding values for the quiescent case cannot be included in this figure because of the choice of the logarithmic scale for the shear rates (their magnitudes are indicated as horizontal lines). It is evident that the crystallization rate is always enhanced by increasing the shear rate. However, the results in terms of $t^{SS}_{0.5}$ (Fig. 8) for the two samples cannot be superposed by vertically shifting of the data from the 0.1PB400 nanocomposite with respect to those from pure PB400. This indicates that the presence of a synergistic effect between the inclusion of MWNT and the applied shear flow. Such an effect can be quantitatively described as follows.

In Fig. 8, the value of the quiescent crystallization half-time, $t^{Q}_{0.5}$, of the pure PB400 can be considered as the reference condition (continuous line). The ratio between $t^{Q}_{0.5}$ for the pure PB400 and the corresponding $t^{Q}_{0.5}$ for the 0.1PB400 nanocomposite (dashed line) is about 1.36, indicating a decrease of 36% in the quiescent crystallization half-time when the 0.1% of MWNT is added to the PB400 matrix. On the other hand, the ratios between $t^{Q}_{0.5}$ and the corresponding $t^{SS}_{0.5}$ values for the pure PB400 are representative of the step-shear flow effect on the crystallization kinetics of the pure matrix. In the case of the applied shear rate of 0.3 s^{-1}, this ratio is about 1.41. A moderate enhancement in the crystallization kinetics is, therefore, recorded since the applied shear flow only corresponds to moderate *We* value (in the range 1.71–3) as discussed earlier. The combined effect of nanotubes and shear flow can be detected by the ratios between PB400 $t^{Q}_{0.5}$ and the corresponding $t^{SS}_{0.5}$ values for the 0.1PB400 sample. It is clear that the combined effect is not additive but synergistic, since for the 0.1PB400 sample at the shear rate of 0.3 s^{-1}, this ratio becomes about 6.5.

A dimensionless overall crystallization constant, k_{SS}/k_Q, representing the overall crystallization constant at a given shear rate divided by the corresponding crystallization constant under quiescent conditions, has been also defined to discuss the enhanced crystallization rate of nanocomposites under flow. As a result, each k_{SS} value reported in Table 3 for the pure matrix and the 0.1PB400 has been normalized with respect to the corresponding k_Q value (as reported in Table 2), where the results (k_{SS}/k_Q *vs* the shear rate plot) are shown in Fig. 9. In this plot, if the combined effects of the nanotube inclusion and the shear flow are additive, then the data for the pure matrix and the nanocomposite should superpose. Clearly, the results show that this event does not occur, while the combined effect is synergistic in nature. The synergistic effect of applied shear and inclusion of fibrous fillers on enhancing the crystallization rate has recently been shown by a combined in situ scattering and diffraction study using synchrotron radiation of semi-crystalline composites [32]. In this synchrotron study, the authors explained that the synergistic effect can be attributed to the interfacial interactions between the shear aligned fibers and the orientation of polymer chains. This may also be the case in this study, where the nanofillers probably provide the pinning points to the surrounding PB chains, thus enhancing their effective relaxation times and the retention of molecular orientation after flow.

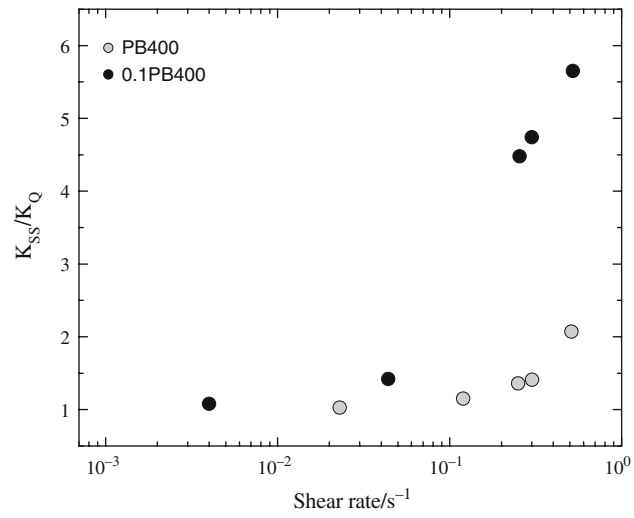

Fig. 9 Normalized overall crystallization rate (k_{SS}/k_Q) as a function of the shear rate for the pure PB400 and the 0.1PB400 nanocomposite. $T_c = 95$ °C

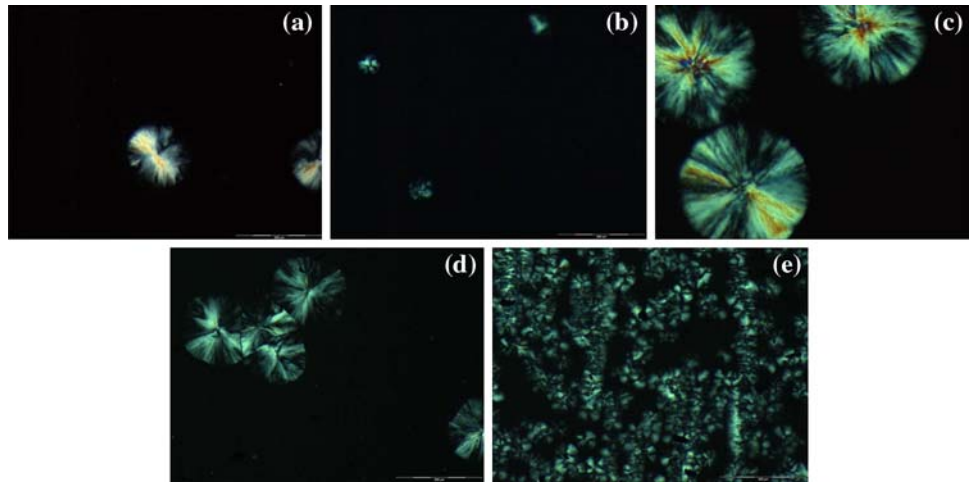

Fig. 10 Optical microscopy images during crystallization at T_c = 95 °C.**a** Pure PB400 in quiescent conditions, at 1,200 s after T_c has been reached; **b** pure PB400 after step-shear flow test (shear rate=0.3 s^{-1}), at 320 s after flow; **c** pure PB400 after step-shear flow test (shear rate=0.3 s^{-1}), at 1200 s after flow; **d** 0.1PB400 nanocomposite in quiescent conditions, at 1,200 s after T_c has been reached; **e** 0.1PB400 nanocomposite after step-shear flow test (shear rate=0.3 s^{-1}), at 320 s after flow. The micrographs refer to a crystallization time of 320 s. The length of the scale bar is 200 μm

Optical microscopic measurements have also been carried out during flow and some selected images are reported in Fig. 10, where the micrographs of the PB400 and the 0.1PB400 crystallizing samples, collected after the application of shear at the rate of 0.3 s^{-1} for 70 s, are shown in Fig. 10b, c, e, respectively; and the corresponding images collected under the quiescent condition as soon as T_c was reached are shown in Fig. 10a, d, respectively. In the case of the pure PB400 crystallized after the step-shear, Fig. 10b, c indicates that the enhanced nucleation rate in spherulitic growth is obtained as a consequence of the applied shear flow. For example, Fig. 10b reveals the morphology at crystallization time of 320 s, above which some spherulites can be detected, after shear flow for PB400 at 95 °C. On the other hand, Fig. 10c refers to crystallization time of 1,200 s after shear, where significant larger spherulites with respect to the quiescent conditions are observed. It is found that PB400 only exhibits an isotropic spherulitic structure, consistent with the expectation of the structure formed at a moderate *We* value between 1.7 and 3.0. This event agrees well with previous literature findings [3, 5–7, 12, 13, 15, 25, 26, 64] that the transition from isotropic spherulitic to rod-like structure occur either at higher *We* value or at higher molecular weights. Finally, in the case of the 0.1PB400 sample, a much higher density of crystallites is seen. These crystallites show a rod-like structure, aligned in the direction of flow, as evident in Fig. 10e. This observation again confirms that the presence of MWNT under flow not only enhances the crystallization kinetic, but also acts as promoters in changing the morphology toward a more anisotropic structure.

Conclusions

In this article, the combined effects of MWNTs inclusion and step-shear flow in isotactic PB were considered. In the quiescent isothermal crystallization, an accelerating effect of MWNT (content from 0.1 to 5 wt%) on the PB crystallization rate was observed, which could be attributed to the nucleating effect of the nanotube on PB. The flow-induced rheological measurements clearly demonstrated that the combined effects of MWNT inclusion and shear flow are not additive but synergistic on enhancing the crystallization rates, which is in agreement with recent findings by a synchrotron scattering and diffraction study [32]. The method of parallel superposition of steady flow and dynamic conditions during the short-time shear flow was particularly suitable to relate the information of molecular orientation during shear flow for both pure PB and nanocomposite samples. It has also been verified that under the moderate *We* number shear flow conditions chosen in this study, only a moderate enhancement in the crystallization kinetics of PB was detected, where the corresponding morphology is isotropic spherulites. A complete different scenario appears when the flow is applied to the nanocomposite. In the case of 0.1 wt% MWNT inclusion (0.1PB400) under the same shear flow conditions, the crystallization rate increases dramatically, where the transition from the isotropic spherulites to a rod-like structure was also seen.

Acknowledgements The US team acknowledges the financial support of this work by National Science Foundation (DMR-0405432).

References

1. Keller A, Kolnaar HWH. Flow-induced orientation and structure formation. In: Meijer HEH, editor. Materials science and technology: a comprehensive treatment. Vol. 18: Processing of polymers. New York: Wiley-VCH; 1997. p. 191–268.
2. Eder G, Janeschitz-Kriegl H. Crystallization. In: Meijer HEH, editor. Materials science and technology: a comprehensive treatment. Vol. 18: Processing of polymers. New York: Wiley-VCH; 1997. p. 269–342.
3. Seki M, Thurman DW, Oberhauser JP, Kornfield JA. Shear-mediated crystallization of isotactic polypropylene: the role of long chain-long chain overlap. Macromolecules. 2002;35:2583–94.
4. Janeschitz-Kriegl H, Ratajski E, Stadlbauer M. Flow as an effective promotor of nucleation in polymer melts: a quantitative evaluation. Rheol Acta. 2003;42:355–64.
5. Hsiao BS, Yang L, Somani RH, Avila-Orta CA, Zhu L. Unexpected shish-kebab structure in a sheared polyethylene melt. Phys Rev Lett. 2005;94:117802–6.
6. Hsiao BS. Role of chain entanglement network on formation of flow-induced crystallization precursor structure. Lect Notes Phys. 2007;714:133–49.
7. Kimata S, Sakurai T, Nozue Y, Kasahara T, Yamaguchi N, Karino T, et al. Molecular basis of the shish-kebab morphology in polymer crystallization. Science. 2007;316:1014–7.
8. Mykhaylyk OO, Chambon P, Graham RS, Fairclough JPA, Olmsted PD, Ryan AJ. The specific work of flow as a criterion for orientation in polymer crystallization. Macromolecules. 2008;41:1901–4.
9. Vleeshouwers S, Meijer HEH. A rheological study of shear induced crystallization. Rheol Acta. 1996;35:391–9.
10. Somani RH, Hsiao BS, Nogales A, Srinivas S, Tsou AH, Sics I, et al. Structure development during shear flow induced crystallization of i-PP: in situ small angle X-ray scattering study. Macromolecules. 2000;33:9385–94.
11. Agarwal PK, Somani RH, Weng W, Mehta A, Yang L, Ran S, et al. Shear-induced crystallization in novel long chain branched polypropylenes by in situ rheo-SAXS and–WAXD. Macromolecules. 2003;36:5226–35.
12. Elmoumni A, Winter HH, Waddon AJ, Fruitwala H. Correlation of material and processing time scales with structure development in isotactic polypropylene crystallization. Macromolecules. 2003;36:6453–61.
13. Elmoumni A, Winter HH. Large strain requirements for shear-induced crystallization of isotactic polypropylene. Rheol Acta. 2006;45:793–801.
14. Bove L, Nobile MR. Shear-induced crystallization of isotactic poly(1-butene). Macromol Symp. 2002;185:135–47.
15. Acierno S, Palomba B, Winter HH, Grizzuti N. Effect of molecular weight on the flow-induced crystallization of isotactic poly(1-butene). Rheol Acta. 2003;42:243–50.
16. Baert J, Van Puyvelde P. Effect of molecular and processing parameters on the flow-induced crystallization of poly-1-butene. Part 1: Kinetics and morphology. Polymer. 2006;47:5871–9.
17. Baert J, Van Puyvelde P, Langouche F. Flow-induced crystallization of PB-1: from the low shear rate region up to processing rates. Macromolecules. 2006;39:9215–22.
18. Dai SC, Qi F, Tanner RI. Strain and strain-rate formulation for flow-induced crystallization. Polym Eng Sci. 2006;46:659–69.
19. Jay F, Haudin JM, Monasse B. Shear-induced crystallization of polypropylenes: effect of molecular weight. J Mater Sci. 1999;34:2089–102.
20. Lagasse RR, Maxwell B. An experimental study of the kinetics of polymer crystallization during shear flow. Polym Eng Sci. 1976;16:189–99.
21. Balzano L, Rastogi S, Peters GWM. Flow induced crystallization in isotactic polypropylene-1, 3:2, 4-bis(3, 4-dimethylbenzylidene)sorbitol blends: implications on morphology of shear and phase separation. Macromolecules. 2008;41:399–408.
22. Byelov D, Panine P, Remerie K, Biemond E, Alfonso GC, de Jeu WH. Crystallization under shear in isotactic polypropylene containing nucleators. Polymer. 2008;49:3076–83.
23. Garcia-Gutierrez MC, Hernandez JJ, Nogales A, Panine P, Rueda DR, Ezquerra TA. Influence of shear on the templated crystallization of poly(butylenes terephthalate)/single wall carbon nanotube nanocomposites. Macromolecules. 2008;41:844–51.
24. Liedauer S, Eder G, Janeschitz-Kriegl H, Jerschow P, Geymayer W, Ingolic E. On the kinetics of shear induced crystallization in polypropylene. Int Polym Proc. 1993;8:236–44.
25. Nogales A, Hsiao BS, Somani RH, Srinivas S, Tsou AH, Balta-Calleja FJ, et al. Shear-induced crystallization of isotactic polypropylene with different molecular weight distributions: in situ small- and wide-angle X-ray scattering studies. Polymer. 2000;42:5247–56.
26. Somani RH, Yang L, Zhu L, Hsiao BS. Flow-induced shish-kebab precursor structures in entangled polymer melts. Polymer. 2005;46:8587–623.
27. Bhattacharyya AR, Sreekumar TV, Liu T, Kumar S, Ericson LM, Hauge RH, et al. Crystallization and orientation studies in polypropylene/single wall carbon nanotube composite. Polymer. 2003;44:2373–7.
28. Anand KA, Agarwal US, Joseph R. Carbon nanotubes induced crystallization of poly(ethylene terephthalate). Polymer. 2006;47:3976–80.
29. Valentini L, Biagiotti J, Kenny JM, Santucci S. Morphological characterization of single-walled carbon nanotubes-PP composites. Compos Sci Technol. 2003;63:1149–53.
30. Kelarakis A, Yoon K, Sics I, Somani RH, Chen X, Hsiao BS, et al. Shear-induced orientation and structure development in isotactic polypropylene melt containing modified carbon nanofibers. J Macromol Sci Phys. 2006;45:247–61.
31. Larin B, Marom G, Avila-Orta CA, Somani RH, Hsiao BS. Orientated crystallization in discontinuous aramid fiber/isotactic polypropylene composites under shear flow conditions. J Appl Polym Sci. 2005;98:1113–8.
32. Larin B, Avila-Orta CA, Somani RH, Hsiao BS, Marom G. Combined effect of shear and fibrous fillers on orientation-induced crystallization in discontinuous aramid fiber/isotactic polypropylene composites. Polymer. 2008;49:295–302.
33. Bove L, Nobile MR. Shear flow effects on polymer melts crystallization: kinetic features. Macromol Symp. 2002;180:169–80.
34. Coppola S, Acierno S, Grizzuti N, Vlassopoulos D. Viscoelastic behavior of semicrystalline thermoplastic polymers during the early stages of crystallization. Macromolecules. 2006;39:1507–14.
35. Acierno S, Grizzuti N, Winter HH. Effects of molecular weight on the isothermal crystallization of poly(1-butene). Macromolecules. 2002;35:5043–8.
36. Azzurri F, Alfonso GC. Lifetime of shear-induced crystal nucleation precursors. Macromolecules. 2005;38:1723–8.
37. Hadinata C, Gabriel C, Rüllmann M, Laun MJ. Comparison of shear-induced crystallization behaviour of PB-1 samples with different molecular weight distribution. J Rheol. 2005;49:327–49.
38. Hadinata C, Gabriel C, Rüllmann M, Kao N, Laun MJ. Shear-induced crystallization of PB-1 up to processing-relevant shear rates. Rheol Acta. 2006;45:539–46.
39. Natta G, Corradini P, Danusso F, Mantica E, Mazzanti G, Pino P, et al. Crystalline high polymers of α-olefins. J Am Chem Soc. 1955;77:1708–10.
40. Petraccone V, Pirozzi B, Frasci A, Corradini P. Polymorphism of isotactic poly-a-butene: conformational analysis of the chain and crystalline structure of form 2. Eur Polym J. 1976;12:323–7.

41. Natta G, Corradini P, Bassi IW. Crystal structure of isotactic poly-alpha-butene. Nuovo Cimento. 1960;15:52–67.
42. Lotz B, Mathieu C, Thierry A, Lovinger AJ, De Rosa C, De Ballesteros OR, et al. Chirality constraints in crystal-crystal transformations: isotactic poly(1-butene) versus syndiotactic polypropylene. Macromolecules. 1998;31:9253–7.
43. Azzurri F, Flores A, Alfonso GC, Sics I, Hsiao BS, Balta Calleja FJ. Polymorphism of isotactic polybutene-1 as revealed by microindentation hardness. Part II: Correlations to microstructure. Polymer. 2003;44:1641–5.
44. Marand H, Xu J, Srinivas S. Determination of the equilibrium melting temperature of polymer crystals: linear and nonlinear Hoffman–Weeks extrapolations. Macromolecules. 1998;31:8219–29.
45. Xu J, Srinivas S, Marand H, Agarwal P. Equilibrium melting temperature and undercooling dependence of the spherulitic growth rate of isotactic polypropylene. Macromolecules. 1998;31:8230–42.
46. Nakamura K, Aoike T, Usaka K, Kanamoto T. Phase Transformation in poly(1-butene) upon drawing. Macromolecules. 1999;32:4975–82.
47. Nobile MR, Bove L, Somma E, Kruszelnicka I, Sterzynski T. Rheological and structure investigation of shear-induced crystallization of isotactic polypropylene. Polym Eng Sci. 2005;45:153–62.
48. Somma E, Valentino O, Titomanlio G, Ianniruberto G. Parallel superposition in entangled polydisperse polymer melts: Experiments and theory. J Rheol. 2007;51:987–1005.
49. Ferry JD. Viscoelastic properties of polymers. Wiley, New York; 1980.
50. Kelarakis A, Mai SM, Booth C, Ryan AJ. Can rheometry measure crystallization kinetics? A comparative study using block copolymers. Polymer. 2005;46:2739–47.
51. Bove L, Nobile MR, Azzurri F, Alfonso GC. Shear-induced crystallization of isotactic polyolefins. In: The 17th annual meeting of the Polymer Processing Society (PPS-17), Montréal, 21–24 May 2001.
52. Iervolino R. Rheology and morphology of the flow induced crystallization in polymers. PhD thesis. University of Salerno, Italy; 2009.
53. Pötschke P, Fornes TD, Paul R. Rheological behavior of multiwalled carbon nanotube/polycarbonate composites. Polymer. 2002;43:3247–55.
54. Pötschke P, Abdel-Goad M, Alig I, Dudkin S, Lellinger D. Rheological and dielectrical characterization of melt mixed polycarbonate-multiwalled carbon nanotube composites. Polymer. 2004;45:8863–70.
55. Du F, Scogna RC, Zhou W, Brand S, Fischer JE, Winey KI. Nanotube networks in polymer nanocomposites: rheology and electrical conductivity. Macromolecules. 2004;37:9048–55.
56. Winter HH, Mours M. Rheology of polymers near liquid-solid transitions. In: Neutron spin echo spectroscopy viscoelasticity rheology. Advances in Polymer Science, vol. 134. Berlin, Germany: Springer; 1997, p. 165–234.
57. Liu C, Zhang J, He J, Hu G. Gelation in carbon nanotube/polymer composites. Polymer. 2003;44:7529–32.
58. Valentino O. The effect of surface treatment and matrix properties on CNT/polymer composites. PhD thesis. University of Salerno, Italy; 2008.
59. Fu Q, Heck B, Strobl G, Thomann Y. A temperature- and molar mass-dependent change in the crystallization mechanism of poly(1-butene): transition from chain-folded to chain-extended crystallization? Macromolecules. 2001;34:2502–11.
60. Baumgartel M, Winter HH. Determination of discrete relaxation and retardation time spectra from dynamic mechanical data. Rheol Acta. 1989;28:511–9.
61. van Meerveld J, Peters GWM, Hutter M. Towards a rheological classification of flow induced crystallization experiments of polymer melts. Rheol Acta. 2004;44:119–34.
62. Nobile MR, Cocchini F. A generalized relation between MWD and relaxation time spectrum. Rheol Acta. 2008;47:509–19.
63. Balzano L, Kukalyekar N, Rastogi S, Peters GWM, Chadwick JC. Crystallization and dissolution of flow-induced precursors. Phys Rev Lett 2008; 100:1–4.
64. Pogodina NV, Lavrenko VP, Srinivas S, Winter HH. Rheology and structure of isotactic polypropylene near the gel point: quiescent and shear induced crystallization. Polymer. 2001;42:9031–43.